C. R. Geoscience 351 (2019) 113–120

Contents lists available at ScienceDirect

Comptes Rendus Geoscience

www.sciencedirect.com

Internal Geophysics (Physics of Earth's Interior)

Synthesis and characterization of polycrystalline $KAlSi_3O_8$ hollandite [liebermannite]: Sound velocities vs. pressure to 13 GPa at room temperature

Ting Chen [a], Gabriel D. Gwanmesia [b,c], Lars Ehm [a,c,d], Charles Le Losq [e], Daniel R. Neuville [f], Brian L. Phillips [a], Baosheng Li [a,c], Robert C. Liebermann [a,c,*]

[a] Department of Geosciences, Stony Brook University, Stony Brook, New York, United States
[b] Department of Physics and Engineering, Delaware State University, Dover, Delaware, United States
[c] Mineral Physics Institute, Stony Brook University, Stony Brook, New York, United States
[d] National Synchrotron Light Source II, Brookhaven National Laboratory, Upton, New York, United States
[e] Research School of Earth Sciences, Australian National University, Canberra, Australia
[f] Institut de Physique du Globe, CNRS, Université Paris-Diderot, Paris-7, 75005 Paris, France

ARTICLE INFO

Article history:
Received 20 March 2018
Accepted after revision 1st October 2018
Available online 14 December 2018

Handled by Guillaume Fiquet

Keywords:
Sound velocities
High pressure
Ultrasonics

ABSTRACT

A polycrystalline specimen of liebermannite [$KAlSi_3O_8$ hollandite] was synthesized at 14.5 GPa and 1473 K using glass starting material in a uniaxial split-sphere apparatus. The recovered specimen is pure tetragonal hollandite [SG: *I4/m*] with bulk density of within 98% of the measured X-ray value. The specimen was also characterized by Raman spectroscopy and nuclear magnetic resonance spectroscopy. Sound velocities in this specimen were measured by ultrasonic interferometry to 13 GPa at room T in a uniaxial split-cylinder apparatus using Al_2O_3 as a pressure marker. Finite strain analysis of the ultrasonic data yielded K_{S0} = 145(1) GPa, K_0' = 4.9(2), G_0 = 92.3(3) GPa, G_0' = 1.6(1) for the bulk and shear moduli and their pressure derivatives, corresponding to V_{P0} = 8.4(1) km/s, V_{S0} = 4.9(1) km/s for the sound wave velocities at room temperature. These elasticity data are compared to literature values obtained from static compression experiments and theoretical density functional calculations.

1. Introduction

Liebermannite is a polymorph of $KAlSi_3O_8$-sanidine, which transforms to the tetragonal hollandite structure [SG: I4/m] at high pressure and temperature (Ringwood et al., 1967). $KAlSi_3O_8$ hollandite is considered to be the most abundant phase in a continental crust composition at pressure and temperature conditions corresponding to the mantle transition zone [400–700 km] (Irifune et al., 1994). Subsequently, Ishii et al. (2012) reported new results on detailed phase relations of continental crust composition as function of pressure and temperature to the conditions of the upperpart of the lower mantle.

The presence of $KAlSi_3O_8$ hollandite in the Earth's interior would make it a possible reservoir of some large ion lithophile (LIL) elements especially in the mantle transition zone and the lower mantle. As ^{40}K is the major radioactive heat source in the Earth's interior and has a significant influence on thermal evolution of the Earth, its behavior in the deep mantle is largely controlled by $KAlSi_3O_8$ hollandite (following Nishiyama et al., 2005).

* Corresponding author at: Stony Brook University, Mineral Physics Institute, Stony Brook, NY 11794-2100, United States.
E-mail address: robert.liebermann@stonybrook.edu (R.C. Liebermann).

https://doi.org/10.1016/j.crte.2018.09.009
1631-0713/

$KAlSi_3O_8$ hollandite is one of several high-pressure phases discovered in the laboratory of A. E. (Ted) Ringwood at the Australian National University; others include majorite garnet and Ca-perovskite (see Fig. 1; from Irifune et al., 1994) in addition to wadsleyite, ringwoodite and bridgmanite for pyrolite compositions. Its stability field has subsequently been studied by quench techniques (Yagi et al., 1994), *in situ* X-ray diffraction experiments (Urakawa et al., 1994) and oxide melt solution calorimetry (Akaogi et al., 2004).

Natural occurrences of $KAlSi_3O_8$ hollandite were first discovered by Langenhorst and Poirier (2000), but these authors did not provide a quantitative structural analysis and thus could not recommend a mineral name to the International Mineralogical Association. Ma et al. (2014) later reported the occurrence of $KAlSi_3O_8$ in the tetragonal hollandite-type structure in the Martian shergottite Zagami and proposed the name of liebermannite for this new mineral [IMA 2013-128], and discussed the implications of this new high-pressure silicate for the Zagami impact event (for complete details, see Ma et al., 2018).

The elastic properties of $KAlSi_3O_8$ hollandite have previously been studied by static compression techniques (Ferroir et al., 2006; Nishiyama et al., 2005; Zhang et al., 1993) and theoretical density functional calculations (Caracas and Boffa Ballaran, 2010; Deng et al., 2011; Kawai and Tsuchiya, 2013; Mookherjee and Steinle-Neumann, 2009). In this paper, we report for the first time, direct measurements of the sound velocities of $KAlSi_3O_8$ hollandite using ultrasonic interferometric techniques in conjunction with large-volume, multi-anvil high-pressure apparatus as developed in our laboratory over the past decade (Li and Liebermann, 2007, 2014; Li et al., 1996a, 1996b, 1998, 2004; Wang et al., 2015). These new elasticity data are compared to literature values obtained from static compression experiments and theoretical density functional calculations.

2. Synthesis of polycrystalline specimen of liebermannite

The synthesis of the glass starting materials was done by Charles Le Losq in the laboratory of Daniel Neuville in the Geomaterial lab at the Institut de Physique du Globe in Paris (IGPP) laboratory by mixing the appropriate amount of Al_2O_3, K_2CO_3 and SiO_2 powders initially dried overnight at 1373 K for SiO_2 and Al_2O_3, and at 623 K for Na_2CO_3 and K_2CO_3. The powder mixtures were crushed in ethanol in an agate mortar for 1 h, and then placed in a Pt crucible. They were heated at ~1 K/min up to 1973 K to ensure a slow decarbonation. After melting at 1973 K, rapid quenches of the melts were performed by dipping the bottom of the Pt crucibles in water. The recovered glasses were crushed again for 1 h in an agate mortar, and melted again at 1973 K. Such cycle of crushing-melting has been repeated 4 times in total, to ensure the synthesis of homogeneous glasses. During the final run, samples were maintained a few hours at 1973 K to obtain bubble-free glasses. Chemical compositions of glasses have been measured using a Cameca SX50 electron microprobe, with a 30 nA current, U = 30 kV, and 5 s of counting. From those measurements, no alkali loss occurred. Raman spectra acquired with a T64000 Jobin-Yvon spectrometer at the IPGP using a 514.532 nm laser focused on fresh surfaces of the samples through a ×100 Olympus objective indicate that the glasses are free from crystals, confirming the initial observations made under an optical microscope (for additional details, see Le Losq and Neuville, 2013; run NAK75.12.12).

Several high-pressure synthesis runs were conducted at various cell pressures and temperatures in large-volume, multi-anvil high-pressure apparatus of the Kawai-type in our laboratory. The experimental conditions were chosen to ensure the synthesis of a pure hollandite polycrystalline specimen suitable for high-frequency ultrasonic interferometric measurements. The most successful run, S-4260, was performed in a 2000-ton, uniaxial split-sphere apparatus (USSA-2000) at pressures of 14.5 GPa and temperature of 1473 K using the NAK75.12.12 glass (see Fig. 2; adapted from Akaogi et al., 2004). After maintaining the maximum pressure and temperature for 3 h, the run was quenched to room temperature (to avoid back

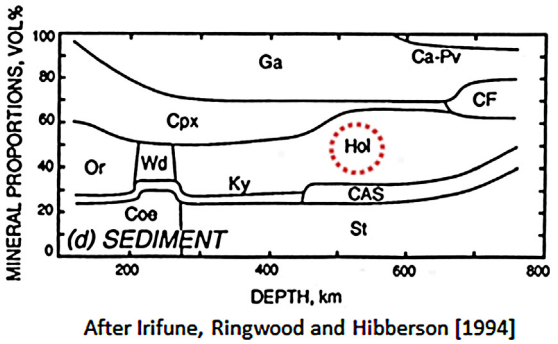

Fig. 1. Phase diagram for terrigenous sediments, whose compositions are basically identical to those of the continental crust [after Irifune et al. (1994)]. Note stability field for $KAlSi_3O_8$ hollandite (Hol). Note: field labelled Wd-wadsleyite is incorrect; correct label should be Wa-wadeite.

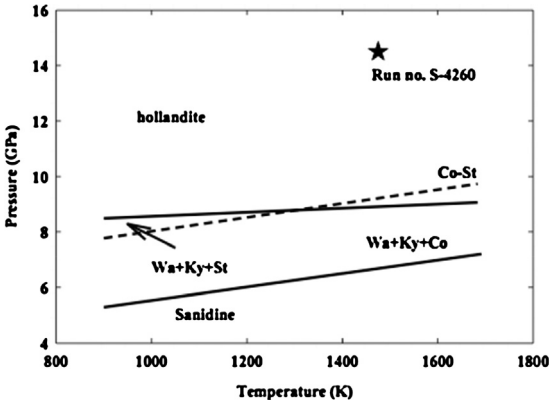

Fig. 2. Phase relations in $KAlSi_3O_8$ (as adapted from Akaogi et al., 2004). Solid lines represent calculated transition boundaries using thermodynamic data, and a dashed line shows the coesite–stishovite transition boundary from Zhang et al. (1996). San: Sanidine; Wa: wadeite; Ky: kyanite; Co: coesite; St: stishovite; Hol: hollandite. Liebermannnite specimen S-4260 was synthesized at 14.5 GPa and 1473 K in a high-pressure run of a duration of 3 h followed by quenching to room temperature and then decompressing.

transformation to sanidine) and then decompressed to room pressure.

3. Characterization of polycrystalline specimen S-4260

X-ray diffraction measurements on the hot-pressed specimen were conducted at sector 13, GSECARS at the Advanced Photon Source at Argonne National Laboratory. Powder diffraction patterns were collected at several spots over the specimen length at a wavelength of 0.31 Å using a MAR165 CCD detector. The two-dimensional diffraction data were transformed into standard patterns using DIOPTAS (Prescher and Prakapenka, 2015). Lattice parameters were obtained from LeBail fits and the structure was refined by the Rietveld method employing the program FULLPROF (Rodriguez-Carvajal, 1990). The background was described by a linear interpolation between fifteen point and the peak profiles were modelled using a pseudo-Voigt function. Six structural parameters were refined, the fractional coordinates x and y for Al/Si, O1 and O2, respectively. The standard deviations of the refined parameters were scaled with the Bérar-factor (Berar and Lelann, 1991).

The observed and calculated diffraction patterns resulting from the Rietveld analysis are shown in Fig. 3. The diffraction pattern contains peaks from a minor impurity (1.5% sanidine presumably formed on back transformation from hollandite on quenching the synthesis run). The refined lattice parameters of $a = 9.329(8)$ Å and $c = 2.725(7)$ Å and structural parameters (Table 1) are in excellent agreement with previously reported data (Yamada et al., 1984; Zhang et al., 1993). Therefore, we are confident about the quality of the synthesized sample for further investigation of the high-pressure elastic properties. The bulk density of the polycrystalline specimen was determined by the Archimedes method to be 3.82 g/cm^3, or 98.0% of the measured X-ray density [3.899 g/cm^3, molar volume 237.15(4) Å^3].

Table 1
Structural parameters of $KAlSi_3O_8$ with hollandite structure. $KAlSi_3O_8$ with hollandite structure crystallizes in the space group I 4/m with the lattice parameters of $a = 9.329(8)$ Å and $c = 2.725(7)$ Å. Cell volume = 237.15(4) Å^3. X-ray density = 3.899 g/cm^3.

Atom	x/a	y/b	z/c
K	0.0	0.0	0.5
Al	0.352(3)	0.168(3)	0.0
Si	0.352(3)	0.168(3)	0.0
O1	0.155(3)	0.204(3)	0.0
O2	0.545(3)	0.165(3)	0.0

The residuals of the Rietveld refinement were R_{Bragg} 4.86% and R_{wp} 14.5%.

Raman spectra for liebermannnite specimen S-4260 were collected on a WITec alpha300R Micro-Imaging Raman Spectrometer using a 532 nm Nd YAG at Stony Brook (Fig. 4). From comparison with hollandite spectra from Beck et al. (2004) and Gillet et al. (2000), we conclude that our specimen is of tetragonal hollandite structure.

Solid-state magic-angle-spinning (MAS) NMR spectra of the synthetic liebermannite specimen S-4260 were acquired at Stony Brook University with a 500 MHz (11.7T) Varian Infinityplus spectrometer operating at 132.2 MHz for ^{27}Al and 99.3 MHz for ^{29}Si. For the ^{29}Si MAS/NMR experiment, the sample was spun at 7 kHz in a Varian/Chemagnetics T3-type probe assembly configured for 5.0 mm (O.D.) rotors. The spectrum was acquired with 4 μs pulses, using a transverse field corresponding to a 5 μs 90 pulse length, and 2000 s relaxation delay for a total of 176 transients. From comparison of the integrated intensity with those of additional spectra obtained with shorter relaxation delays, we estimate the ^{29}Si spin-lattice relaxation time to be approximately 600 s. The ^{27}Al spectrum was acquired at a spinning rate of 15 kHz using a probe assembly configured for 4 mm (O.D.) rotors. The single-pulse excitation consisted of 0.5 μs pulses, where

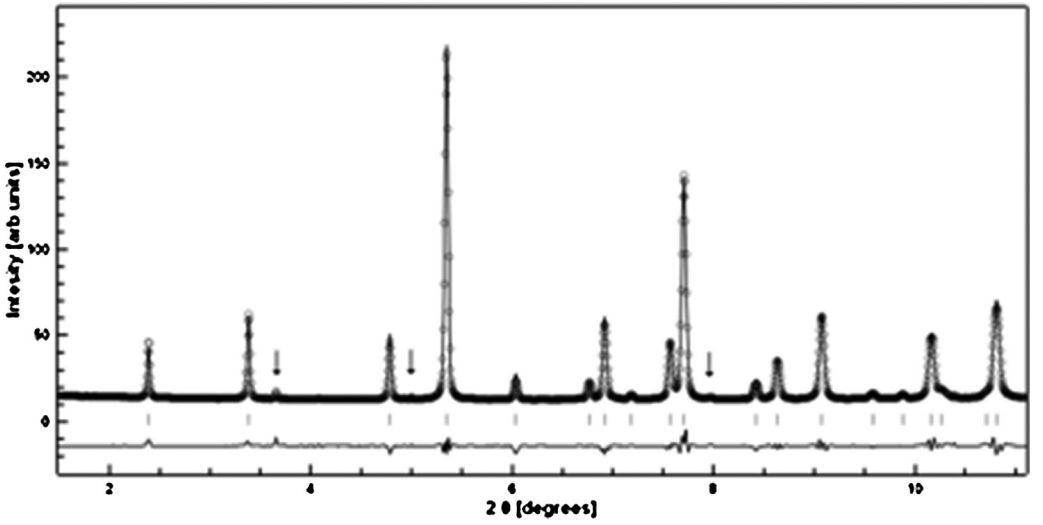

Fig. 3. Observed (○) and calculated (line) diffraction pattern of liebermannite specimen S-4260. The difference curve of the fit is shown below the patterns. The arrows indicate the contributions of a minor impurity to the diffraction data (1.5% sanidine presumably formed on back transformation from hollandite on quenching the synthesis run).

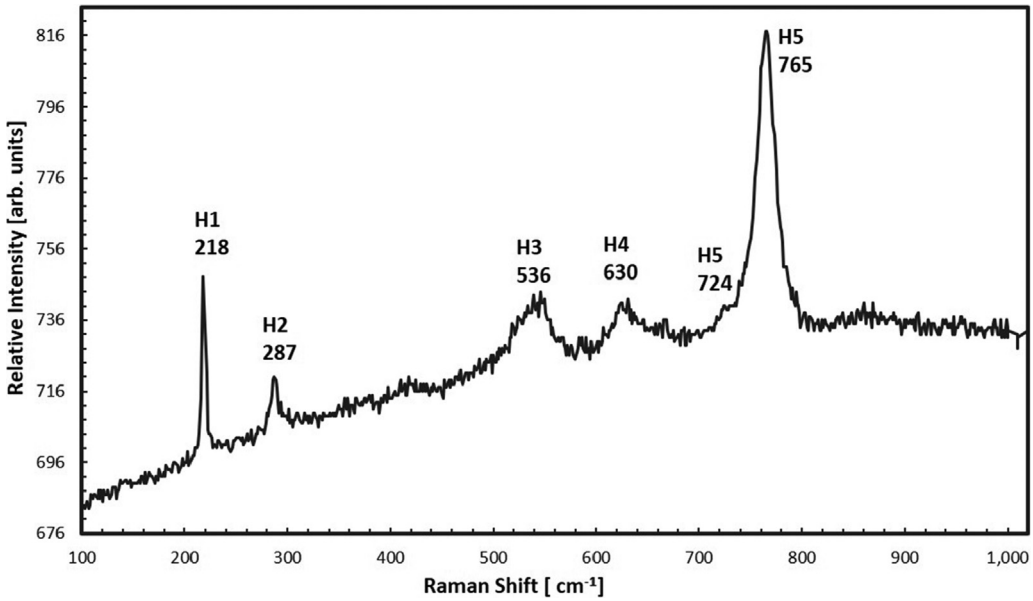

Fig. 4. Raman spectra for liebermannite specimen S-4260. Peaks are labelled following Beck et al. (2004) spectra for synthetic hollandite; all peak positions are within 3% of those Beck et al., most within 0.4%.

the non-selective 90° pulse length was 4.5 μs, and a 5 s relaxation delay for a total of 30,000 scans. To help constrain the range of quadrupolar coupling parameters, an additional spectrum was acquired under similar conditions on a 400 MHz (9.4T) Varian Inova spectrometer using the same probe assembly. Chemical shifts are reported relative to external standards of tetramethylsilane for ^{29}Si and a 0.1 *m* $AlCl_3$ solution for ^{27}Al.

The NMR spectra for both ^{29}Si (Fig. 5a) and ^{27}Al (Fig. 5b) contain single, asymmetrical peaks consistent with a disordered arrangement of Si and Al in the single octahedral site of liebermannite, and absence of major impurities. The peak in the ^{29}Si MAS/NMR spectrum occurs at −185.1 ppm with a full-width at half-maximum (FWHM) of 2.3 ppm. The asymmetry is evident as a slight tail toward more positive chemical shifts, resulting in a weighted average chemical shift of −184.7 ppm, offset from the peak position. Alternatively, the spectrum can be fit well with two Gaussian curves consisting of a narrower peak at −185.2 ppm, 1.6 ppm FWHM, plus a broader curve at −184.4 ppm, 3.7 ppm FWHM, having an approximate intensity ratio 0.4:0.6. An additional small feature appears to be present near −187.7 ppm that could be fit with a Gaussian curve with a width of 0.7 ppm FWHM and representing less than 1% of the integrated intensity. However, the associated structure is close in amplitude to that of the spectral noise and might be an artifact. The observed ^{29}Si chemical shift falls well within the range of those previously reported for six-coordinated Si (e.g., Griffin and Ashbrook, 2013), and in particular for dense high-pressure aluminosilicates containing edge-shared octahedra (Xue et al., 2006, 2009, 2010). However, in contrast to these previous studies the present results do not show distinct spectral features for Si octahedra with differing Si, Al configurations in the adjacent edge-shared octahedra. This result suggests that for the liebermannite structure, the range of ^{29}Si chemical shifts for each type of configuration is of the same order or larger than the change in chemical shift with substitution of Si for Al in neighboring octahedra.

The liebermannite specimen yields a ^{27}Al MAS/NMR spectrum (Fig. 5b) that is dominated by an asymmetric center-band, positioned at 8.1 ppm with a width of 8.5 ppm FWHM under the experimental conditions (11.7T). An additional minor peak is present near +56 ppm, containing less than 0.5% of the center-band intensity and not apparent at the scale of Fig. 5b, that suggests the impurity observed in the XRD data contains tetrahedral Al. The asymmetry of the main peak manifests as a sharper edge at higher chemical shift and a tail that extends toward lower chemical shifts. As a number of studies have noted (e.g., Coster et al., 1994; Jager et al., 1993), such a peak shape for quadrupolar nuclei is typically observed in disordered materials and is characteristic of a distribution of quadrupolar coupling interactions where the range of chemical shifts is small compared to the quadrupolar broadening. The observed peak shape can be well fitted with an isotropic chemical shift of 11.0 ppm and a Gaussian distribution of electric field gradients having a mean quadrupolar coupling constant (Cq) of 3.7 MHz and FWHM Cq of 4.1 MHz. The fit of the peak was accomplished with a laboratory-built program based on the method described by Coster et al. (1994), but which is similar in effect to the Gaussian isotropic model (e.g., Neuville et al., 2004). In terms of isotropic chemical shift, average Cq value, and peak asymmetry resulting from a broad Cq distribution, the present results for liebermannite closely resemble those for other dense octahedral aluminosilicates containing edge-shared octahedra such as phase "egg", topaz–OH II, and high-pressure $CaAl_4Si_2O_{11}$ (Xue et al., 2006, 2009, 2010).

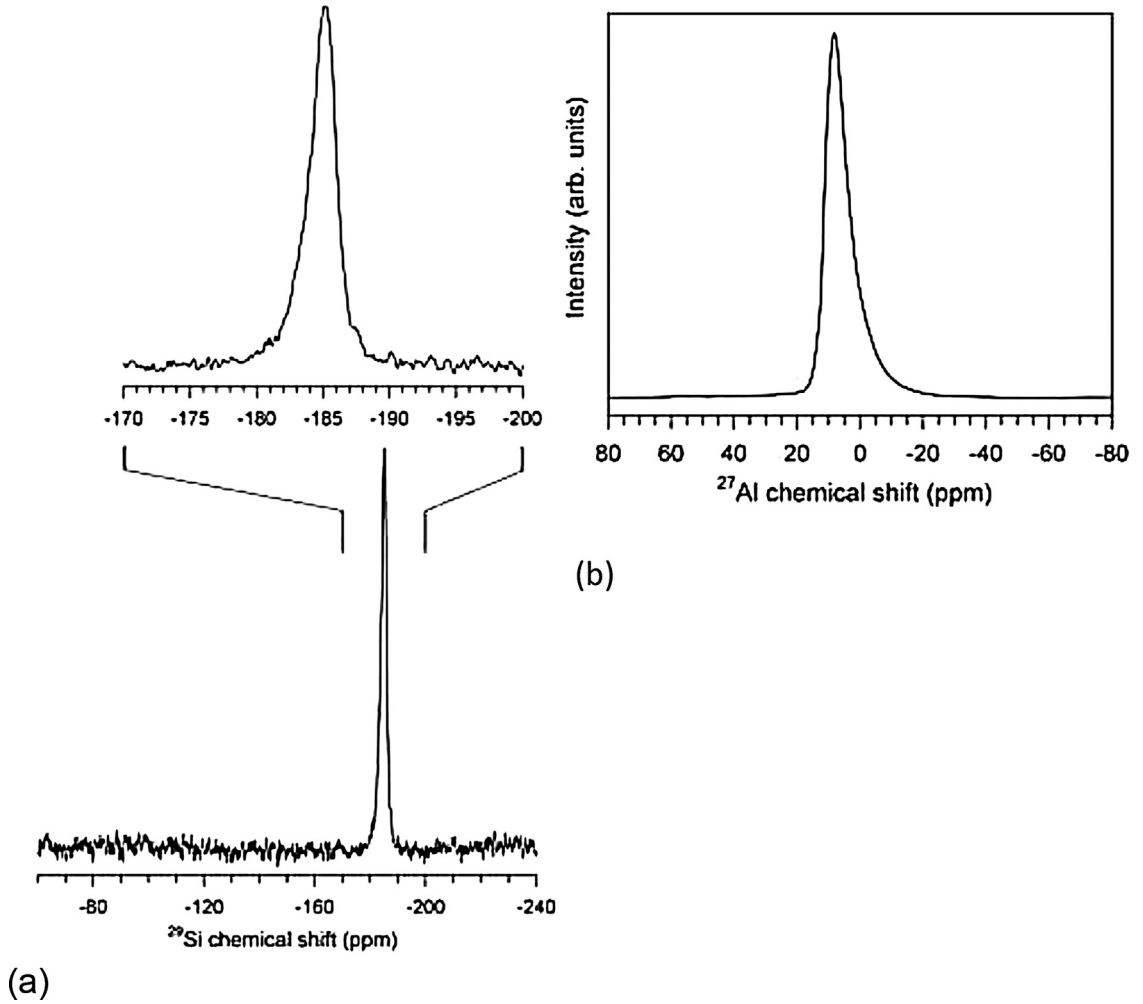

Fig. 5. MAS/NMR spectra for the synthetic liebermannite specimen S-4260: a: ^{29}Si spectrum, acquired at a 7 kHz spinning rate and 2000 s relaxation delay for 176 acquisitions. *Bottom*: full chemical shift range for silicates; *Top*: expanded view of the observed peak; b: center-band region of the ^{27}Al MAS/NMR spectrum, obtained at 11.7 T with a 15 kHz spinning rate, 0.5 μs pulses, and 5 s relaxation delay for 30,000 acquisitions. A broad manifold of satellite transition spinning sidebands exists beyond the displayed spectral region.

4. Ultrasonic experiments

High-pressure acoustic velocities on the liebermannite sample were measured in a 1000-ton uniaxial split-cylinder apparatus (USCA-1000) up to 13.0 GPa at room temperature. A dual mode $LiNbO_3$ transducer (10 rotated Y-cut) was mounted on the back of the tungsten carbide anvil to generate and receive both P and S waves simultaneously. The sample sat roughly in the center of the cell surrounded by a BN sleeve. A disk of alumina with 3.759(1) mm in length and 3.160(1) mm in diameter was used as the buffer rod to propagate acoustic waves into the sample, and also served as an *in situ* pressure calibrant (Wang et al., 2015). On the other end of the sample, NaCl and Pb disks were inserted to provide a pseudo-hydrostatic environment under pressure. A thin gold layer (~2 μm) was placed on the two ends of the sample as well as between the buffer rod and the anvil to enhance the mechanical coupling and to optimize the energy of the acoustic waves propagating into the sample. Two-way travel times in the sample were obtained using pulse echo overlap (PEO) method by overlapping the signals reflected from the front and end surfaces of the sample (Li et al., 2002). Perturbations from the gold foil to travel times were corrected following the procedure of Niesler and Jackson (1989).

The results of these ultrasonic experiments are plotted in Fig. 6. The travel times (Fig. 6a) for both compressional [P] and shear [S] waves decrease systematically with increasing pressure; note that the travel times below 2 GPa are longer, presumably due to incomplete coupling of the buffer rod and specimen during initial loading (see also Li et al., 1996a, 1996b). For this reason, these two data points were not included in the subsequent fitting process. The sample was considered to have undergone pseudo-hydrostatic compression given the small length changes (within 0.24%) observed after recovery from the USCA-1000. Thus the sample lengths can be derived from the method developed by Cook (1957). Using the calculated length changes (Fig. 6b), the velocities of P and S waves are

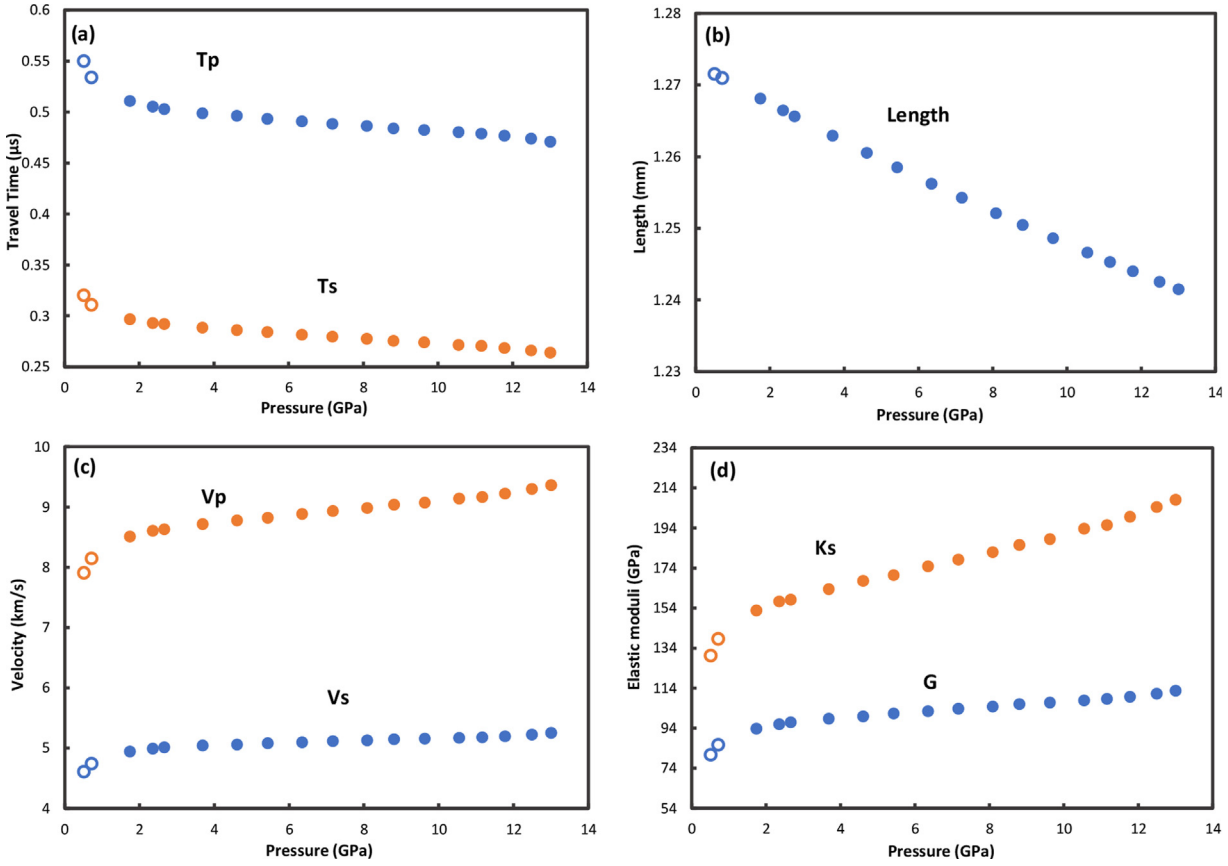

Fig. 6. Results of ultrasonic experiments on S-4260 liebermannite specimen up to 13.0 GPa at room temperature. Open circles: data at low pressures, which are not used in the fitting process. Closed circles: data used for equation of state fitting: a: travel times of compressional [P] and shear [S] waves vs. pressure; b: length change vs. pressure; c: compressional [V_p] and shear [V_s] wave velocities vs. pressure; d: adiabatic bulk [K_s] and shear [G] moduli vs. pressure.

shown in Fig. 6c. With densities inferred from the length change data $\left[\frac{\rho_0}{\rho} = \left(\frac{l}{l_0}\right)^3\right]$, the bulk $\left[K_S = \rho V_P^2 - \frac{4}{3}\rho V_S^2\right]$ and shear $\left[G = \rho V_S^2\right]$ moduli are calculated and shown in Fig. 6d.

By fitting to a third-order Eulerian finite strain equation of state (Niesler and Jackson, 1989), the ultrasonic data in Fig. 6 are used to calculate the zero-pressure moduli and velocities as well as their pressure derivatives, yielding K_{S0} = 145(1) GPa, K_0' = 4.9(2), G_0 = 92.3(3) GPa, G_0' = 1.6(1), V_{P0} = 8.4(1) km/s, V_{S0} = 4.9(1) km/s, dV_p/dP = 0.068 km/s/GPa, dV_s/dP = 0.022 km/s/GPa (Table 2).

5. Comparison of elastic properties of $KAlSi_3O_8$ hollandite obtained in this study with those from the literature

In Table 3, we compare various experimental measurements of the elasticity of $KAlSi_3O_8$ hollandite with calculations from density functional theory. The experimental data were obtained at 300K, whereas most of the DFT calculations are for the 0K static lattice. Our values of K_0 and K_0' are lower/higher, respectively than those from the isothermal compression experiments; this may be partly explained by the fact that K_0' is constrained to be 4.0 in the fitting of the PV data to the Birch–Murnaghan equation of state (third-order Eulerian finite strain equation of state). If we fit our data with a fourth-order equation of state, we obtain K_0 = 148 GPa (unchanged from third-order) and K_0' = 3.1 (much lower even than previous PVT experiments).

It is unlikely that our low values of K_0 are due to uncertainties in the measurements of sample length. To verify this, we have used the values of K_0 = 183 GPa and K_0' = 4.0 from Nishiyama et al. (2005) to calculate the lengths in the ultrasonic experiments; the resultant velocities are within 0.43% of those shown in Fig. 6.

Table 2
Elasticity of $KAlSi_3O_8$ hollandite: calculated bulk [K] and shear [G] moduli during compression (using Cook's method to obtain the sample length)[a].

		This study
K_0	GPa	145(1)
K_0'		4.9(2)
G_0	GPa	92.3(3)
G_0'		1.6(1)
V_{p0}	km/s	8.4(1)
V_{s0}	km/s	4.9(1)
dV_p/dP	km/s/GPa	0.068
dV_s/dP		0.022

[a] Data points below 2 GPa were ignored in the fitting process.

Table 3
Elasticity of $KAlSi_3O_8$ hollandite from experimental measurements and theoretical calculations.

Reference	V_0	K_0	K_0'	G_0	G_0'	V_p	V_s
	Å^3	GPa		GPa		km/s	
Experimental							
This study							
Finite strain[b]	237	145	4.9	92.3	1.6	8.4	4.9
Finite strain[c]	237	148	3.1				
Zhang et al. (1993) PV	236	180(3)	4.0[a]				
	[V_0 free]	191	4.0[a]				
Nishiyama et al. (2005) PVT	238	183(3)	4.0[a]				
Ferroir et al. (2006) PV	237	201	4.0[a]				
Theoretical							
Mookherjee and Steinle-Neumann (2009) DFT–LDA							
EOS static	228	225	4.3				
EOS 300K	232	212	4.3				
Elastic	228	232	4.1	134	1.0	10.1	5.75
Caracas and Boffa Ballaran (2010) DFT-LDA	225	224		143		10.19	5.98
Deng et al. (2011) DFT-GGA	245	174	3.99				
Kawai and Tsuchiya (2013) DFT-LDA	234	205	4.18			9.46	5.28

PV: static compression at high P; PVT: static compression at high P and T; DFT: density functional theory; LDA: local density approximation; GGA: generalized gradient approximation; Static 0K; EOS: Equation of state P–V.
[a] K_0' fixed in Birch–Murnaghan equation.
[b] Eulerian finite strain fitting to ultrasonic data: 3rd order.
[c] Eulerian finite strain fitting to ultrasonic data: 4th order: $K_0'' = 0.023$ GPa^{-1}.

According to Gerd Steinle-Neumann (personal communication), the difference between the measured K_0 and G_0 and those calculated (for example by Mookherjee and Steinle-Neumann, 2009) is unlikely to be due to the difference in temperature as their calculations show that K_0 is reduced from 225 to 212 from 0K to 300K. Some of the differences in K_0 reported for the DFT calculations may be due to the different cell volumes adopted by the authors (e.g., compare those from Mookherjee and Steinle-Neumann, 2009 and Caracas and Boffa Ballaran, 2010 with those from Deng et al., 2011 and Kawai and Tsuchiya, 2013). Resolution of the reasons for the discrepancies between experimental (ultrasonics, static compression) and theoretical calculations requires further investigations.

Acknowledgements

This paper is a special endeavor for the corresponding author (RCL), as he has worked with both the first person to synthesize $KAlSi_3O_8$ hollandite in the laboratory (Ted Ringwood) and the first person to discover it in nature (Jean-Paul Poirier, with Falko Langenhorst). He would like to dedicate this paper to Jean-Paul Poirier, whom he first met in 1981 at the 2nd Japan–US Seminar on High-pressure Research in Hakone, Japan and later spent a profitable sabbatical leave in Poirier's Geomaterial laboratory at the IPGP in Paris in 1984.

We thank Timothy Glotch and Melinda Rucks for access and assistance with the Raman spectroscopic measurements at Stony Brook. We thank Steeve Greaux, Tetsuo Irifune, Chi Ma, Gerd Steinle-Neumann and Oliver Tschauner for discussions of this research project. We appreciate the constructive comments and suggestions of Masaki Akaogi and an anonymous reviewer.

This research was supported by the National Science Foundation via grants EAR 15-24078 to Li and Liebermann and EAR 14-17024 to Gwanmesia. Support for the solid-state NMR facilities at Stony Brook during the course of this study was provided in part by NSF grant EAR 1249696 to Phillips. Use of the COMPRES Cell Assembly Project was supported by COMPRES under Cooperative Agreement EAR 16-61511.

We thank Vitali Prakapenka and Clemens Prescher for providing the X-ray diffraction data, which were obtained at GeoSoilEnviroCARS (The University of Chicago, Sector 13), Advanced Photon Source (APS), Argonne National Laboratory. GSECARS is supported by the National Science Foundation – Earth Sciences (EAR – 1634415) and Department of Energy-GeoSciences (DE-FG02-94ER14466). This research used resources of the Advanced Photon Source, a US Department of Energy (DOE) Office of Science User Facility operated for the DOE Office of Science by Argonne National Laboratory under Contract No. DE-AC02-06CH11357.

References

Akaogi, M., Kamii, N., Kishi, A., Kojitani, H., 2004. Calorimetric study of high-pressure transitions in $KAlSi_3O_8$. Phys. Chem. Miner. 31, 85–91.
Beck, P., Gillet, P., Gautron, L., Daniel, I., El Goresy, A., 2004. A new natural high-pressure (Na,Ca)-hexaluminosilicate $[(Ca_xNa_{1-x})Al_3 + xSi_{3-x}O_{11}]$ in shocked Martian meteorites. Earth Planet. Sci. Lett. 219, 1–12.
Berar, J.-F., Lelann, P., 1991. E.s.d.'s and estimated probable error obtained in Rietveld refinements with local correlations. J. Appl. Crystallogr. 24, 1–5.
Caracas, R., Boffa Ballaran, T., 2010. Elasticity of (K,Na)$AlSi_3O_8$ hollandite from lattice dynamics calculations. Phys. Earth Planet. Inter. 181, 21–26 (297).
Cook, R.K., 1957. Variation of elastic constants and static strains with hydrostatic pressure: a method for calculation from ultrasonic measurements. J. Acoust. Soc. Am. 29, 445–449.

Coster, D., Blumenfeld, A.L., Fripiat, J.J., 1994. Lewis acid sites and surface aluminum in aluminas and zeolites: a high-resolution NMR study. J. Phys. Chem. 98, 6201–6621.

Deng, L., Liu, X., Liu, H., Zhang, Y., 2011. A first-principles study of the phase transition from Holl-I to Holl-II in the composition $KAlSi_3O_8$. Am. Mineral. 96, 974–982.

Ferroir, T., Onozawa, T., Yagi, T., Merkel, S., Miyajima, N., Nishiyama, N., Irifune, T., Kikegawa, T., 2006. Equation of state and phase transition in $KAlSi_3O_8$ hollandite at high-pressure. Am. Mineral. 91, 327–332.

Gillet, P., Chen, M., Dubrovinsky, L., El Goresy, A., 2000. Natural $NaAlSi_3O_8$ hollandite in the shocked Sixiangkou meteorite. Science 287, 1633–1636.

Griffin, J.M., Ashbrook, S.E., 2013. Solid-state NMR of high-pressure silicates in the Earth's mantle. In: Webb, G.A. (Ed.), Annual Reports on NMR Spectroscopy, Elsevier Publishing, Oxford, UK, 2013, 79, 241-332., 79, Elsevier Publishing, Oxford, United Kingdom, pp. 241–332.

Irifune, T., Ringwood, A.E., Hibberson, W.O., 1994. Subduction of continental crust and terrigenous and pelagic sediments: an experimental study. Earth Planet. Sci. Lett. 126, 3510368.

Ishii, T., Kojitani, H., Akaogi, M., 2012. High-pressure phase transitions and subduction behavior of continental crust at pressure-temperature conditions up to the upper part of the lower mantle. Earth Planet. Sci. Lett. 357–358, 31–41.

Jager, C., Kunath, G., Losso, P., Scheler, G., 1993. Determination of distributions of the quadrupole interaction in amorphous solids by ^{27}Al satellite transition spectroscopy. Solid State Nucl. Magn. Reson. 2, 73–82.

Kawai, K., Tsuchiya, T., 2013. First-principles study on the high-pressure phase transition and elasticity of $KAlSi_3O_8$ hollandite. Am. Mineral. 98, 207–218.

Langenhorst, F., Poirier, J.-P., 2000. 'Eclogitic' minerals in a shocked basaltic meteorite. Earth Planet. Sci. Lett. 176, 259–265.

Le Losq, C., Neuville, D.R., 2013. Effect of the Na/K mixing on the structure and rheology of silica-rich melts. Chem. Geol. 346, 57–71.

Li, B., Liebermann, R.C., 2007. Indoor seismology by probing the Earth's interior by using sound velocity measurements at high-pressures and temperatures. Proc. Natl. Acad. Sci. USA 104, 9145–9150.

Li, B., Liebermann, R.C., 2014. Study of the Earth's interior using measurements of sound velocities in minerals by ultrasonic interferometry. Phys. Earth Planet. Inter. 233, 135–153.

Li, B., Jackson, I., Gasparik, T., Liebermann, R.C., 1996a. Elastic wave velocity measurement in multi-anvil apparatus to 110 GPa using ultrasonic interferometry. Phys. Earth Planet. Inter. 98, 79–91.

Li, B., Chen, G., Gwanmesia, G.D., Liebermann, R.C., 1998. Sound velocity measurements at mantle transition zone conditions of pressure and temperature using ultrasonic interferometry in a multi-anvil apparatus. In: Manghnani, M.H., Syono, Y., Yagi, T. (Eds.), Properties of Earth and Planetary Materials at High-pressure & Temperatures. American Geophysical Union, Washington, D. C., pp. 41–61.

Li, B., Chen, K., Kung, J., Liebermann, R.C., Weidner, D.J., 2002. Sound velocity measurement using transfer function method. Proc. AIRAPT Conference, Beijing, July 2001. J. Phys. Condens. Matter 14, 11337–11342.

Li, B., Kung, J., Liebermann, R.C., 2004. Modern techniques in measuring elasticity of Earth materials at high-pressure and high temperature using ultrasonics in conjunction with synchrotron X-radiation. Phys. Earth Planet. Inter. 143–144, 559–574.

Li, B., Rigden, S.M., Liebermann, R.C., 1996b. Elasticity of stishovite at high-pressure. Phys. Earth Planet. Inter. 96, 113–127.

Ma, C., Tschauner, O., Beckett, J.R., 2014. Liebermannite, IMA 2013-128. CNMNC Newsletter No. 20, June 2014, p. 551. Miner. Mag. 78, 549–558.

Ma, C., Tschauner, O., Beckett, J.R., Rossman, G.R., Prescher, C., Prakapenke, V.B., Bechtel, H.A., McDowell, A., 2018. Liebermannite, $KAlSi_3O_8$, a new shock-metamorphic, high-pressure mineral from the Zagami Martian meteorite. Meteorit. Planet. Sci. 53, 50–61, http://dx.doi.org/10.1111/maps.13000.

Mookherjee, M., Steinle-Neumann, G., 2009. Detecting deeply subducted crust from the elasticity of hollandite. Earth Planet. Sci. Lett. 288, 349–358.

Neuville, D.R., Cormier, L., Massiot, D., 2004. Al environment in tectosilicate and peraluminous glasses: a ^{27}Al MQ-MAS NMR, Raman, and XANES investigation. Geochim. Cosmochim. Acta 68, 5071–5079.

Niesler, H., Jackson, I., 1989. Pressure derivatives of elastic wave velocities from ultrasonic interferometric measurements on jacketed polycrystals. J. Acoust. Soc. Am. 86, 1573–1585.

Nishiyama, N., Rapp, R., Irifune, T., Sanehira, T., Yamazaki, D., Funakoshi, K., 2005. Stability and P-V-T equation of state $KAlSi_3O_8$ hollandite determined by in situ X-ray observations and implications for dynamics of subducted continental crust material. Phys. Chem. Miner. 32, 627–637.

Prescher, C., Prakapenka, V.B., 2015. DIOPTAS: a program for reduction of two-dimensional X-ray diffraction data and data exploration. High Pressure Res. 35, 223–230.

Ringwood, A.E., Reid, A.F., Wadsley, A.D., 1967. High-pressure $KAlSi_3O_8$, an aluminosilicate with sixfold coordination. Acta Crystallogr. 23, 1093–1095.

Rodriguez-Carvajal, J., 1990. Fullprof: a program for Rietveld refinement and pattern matching analysis. In: Abstracts of the Satellite Meeting on Powder Diffraction of the XVth Congress of the International Union of Crystallography, Toulouse, France.

Urakawa S., Kondo T., Igawa N., Shimomura O., and Ohno H., Synchrotron radiation study on the high-pressure and high-temperature phase relations of $KAlSi_3O_8$, Phys. Chem. Minerals, 21, 1994, 387–391,

Wang, X., Chen, T., Qi, X., Zou, Y., Kung, J., Yu, T., Wang, Y., Liebermann, R.C., Li, B., 2015. Acoustic travel time gauges for in situ determination of pressure and temperature in multi-anvil apparatus. J. Appl. Phys. 118, 065901.

Xue, X.Y., Kanzaki, M., Fukui, H., Ito, E., Hashimoto, T., 2006. Cation order and hydrogen bonding of high-pressure phases in the Al_2O_3–SiO_2–H_2O system: an NMR and Raman study. Am. Mineral. 91, 850–861.

Xue, X.Y., Kanzaki, M., Fukui, H., 2010. Unique crystal chemistry of two polymorphs of topaz-OH: a multi-nuclear NMR and Raman study. Am. Mineral. 95, 1276–1293.

Xue, X.Y., Zhai, S.M., Kanzaki, M., 2009. Si-Al distribution in high-pressure $CaAl_4Si_2O_{11}$ phase: A ^{29}Si and ^{27}Al NMR study. Am. Mineral. 94, 1739–1742.

Yagi, A., Suzuki, T., Akaogi, M., 1994. High-pressure transitions in the system $KAlSi_3O_8$–$NaAlSi_3O_8$. Phys. Chem. Miner. 21, 12–17.

Yamada, H., Matsui, Y., Ito, E., 1984. Crystal-chemical characterization of $KAlSi_3O_8$ with the hollandite structure. Mineral. J. 12, 29–34.

Zhang, J., Ko, J., Hazen, R.M., Prewitt, C.T., 1993. High-pressure crystal chemistry of $KAlSi_3O_8$ hollandite. Am. Mineral. 78, 493–499.

Zhang, J., Li, B., Utsumi, W., Liebermann, R.C., 1996. In situ X-ray observations of the coesite–stishovite transition: reversed phase boundary and kinetics. Phys. Chem. Miner. 23, 1–10.